

DMFT+ Σ APPROACH TO DISORDERED HUBBARD MODEL*E. Z. Kuchinskii*^{*}, *M. V. Sadovskii*^{**}*Institute for Electrophysics, Russian Academy of Sciences, Ural Branch
620016, Ekaterinburg, Russia**Mikheev Institute for Metal Physics, Russian Academy of Sciences, Ural Branch
620990, Ekaterinburg, Russia*

Received July 6, 2015

We briefly review the generalized dynamic mean-field theory DMFT+ Σ applied to both repulsive and attractive disordered Hubbard models. We examine the general problem of metal–insulator transition and the phase diagram in the repulsive case, as well as the BCS–BEC crossover region of the attractive model, demonstrating a certain universality of single-electron properties under disordering in both models. We also discuss and compare the results for the density of states and dynamic conductivity in the repulsive and attractive cases and the generalized Anderson theorem behavior of the superconducting critical temperature in the disordered attractive case. A brief discussion of the behavior of Ginzburg–Landau coefficients under disordering in the BCS–BEC crossover region is also presented.

Contribution for the JETP special issue in honor of L. V. Keldysh's 85th birthday

DOI: 10.7868/S0044451016030111

1. INTRODUCTION

Strongly correlated electronic systems, which are mainly realized in a range of compounds containing transition or rare-earth elements with partially filled $3d$, $4f$, or $5f$ shells, attract attention of scientists because of their unusual physical properties and are notorious for major difficulties in theoretical description. Perhaps the most significant development in this area has been the discovery of high-temperature superconductivity in copper oxides, which are considered a typical example of strongly correlated systems.

Early qualitative ideas formulated mainly by Mott [1] as well as the introduction of the seminal model by Hubbard [2] inspired hundreds of theoretical papers, which now constitute a separate branch of condensed matter theory. Probably the most impressive achievement in this field in recent years was the development of dynamical mean-field theory (DMFT), which provides an asymptotically exact solution of the Hubbard model in the limit of infinitely many dimensions [3–8].

Most of the studies of strongly correlated systems within the Hubbard model are devoted to the case of repulsive interactions among electrons, which are directly related to many topical problems, with most attention paid to the physics of high- T_c superconductivity in cuprates and the general problem of the metal–insulator transition in cuprates and other similar oxides of transition metals.

Another direction of research is the studies of the Hubbard model with attractive interaction, which is related mainly to a rather old problem of strong-coupling superconductivity, especially to the theoretical description of the notorious BCS-to-BEC (Bardeen–Cooper–Schrieffer to Bose–Einstein condensation) crossover, which is also directly related to the problem of high- T_c superconductivity in copper oxides. Starting with pioneering papers by Eagles and Leggett [9, 10] at $T = 0$ and the important progress achieved by Nozières and Schmitt-Rink [11], who suggested an effective method to study the transition temperature crossover region, this field has produced a large number of theoretical papers published during the recent years, including successful applications of the DMFT approach.

This last area of research is also directly connected with recent progress in experimental studies of quantum gases in magnetic and optical dipole traps, as well

* E-mail: Kuchinsk@iep.uran.ru

** E-mail: Sadovski@iep.uran.ru

as in optical lattices, with controllable parameters, such as the density and interaction strength (cf. reviews [12, 13]), which has increased the interest in superconductivity (superfluidity of fermions) with a strong pairing interaction, including the BCS–BEC crossover region.

In recent years, we have developed the so-called generalized DMFT+ Σ approach [14–17], which is very convenient for the studies of different additional interactions in the repulsive Hubbard model, such as pseudogap fluctuations [14–17], disorder [18, 19], electron–phonon interaction [20], and so on. This approach is also well suited to the analysis of two-particle properties, such as the optical (dynamic) conductivity [18, 21]. In Ref. [22], we used this approximation to calculate single-particle properties of the normal phase and optical conductivity in the attractive Hubbard model. Recently, we used the DMFT+ Σ approach to study disorder influence on the superconducting transition temperature in this model [23, 24].

Below, we concentrate on a discussion the of disorder effects in both repulsive and attractive Hubbard models. There are not so many works devoted to the studies of disorder effects in Hubbard models, because of many theoretical complications related to the problem of the interplay of disorder scattering and Hubbard interaction. We concentrate exclusively on our DMFT+ Σ approach, which is actually very convenient here and provides a good interpolation scheme between different limit cases. We discuss the results obtained in our previous work, and similarities and dissimilarities of disorder effects in repulsive and attractive Hubbard models, in some cases demonstrating universal dependences on disorder.

2. BASICS OF THE DMFT+ Σ APPROACH TO DISORDERED SYSTEMS

The Hamiltonian of a disordered Hubbard model can be written as

$$H = -t \sum_{\langle ij \rangle \sigma} a_{i\sigma}^\dagger a_{j\sigma} + \sum_{i\sigma} \epsilon_i n_{i\sigma} + U \sum_i n_{i\uparrow} n_{i\downarrow}, \quad (1)$$

where $t > 0$ is the transfer integral between nearest sites of the lattice, U is the onsite interaction ($U > 0$ in the case of repulsive interaction, and $U < 0$ in the case of attraction), $n_{i\sigma} = a_{i\sigma}^\dagger a_{i\sigma}$ is the operator of the number of electrons on lattice site i , $a_{i\sigma}$ ($a_{i\sigma}^\dagger$) is the annihilation (creation) operator for the electron with spin σ on site i . The local energy levels ϵ_i are assumed to be independent random variables at different lattice

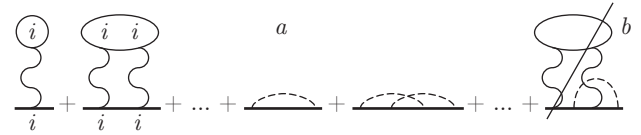


Fig. 1. Typical “skeleton” self-energy diagrams in the DMFT+ Σ approximation

sites (Anderson disorder) [25]. To simplify the diagram technique in what follows, we assume the Gaussian distribution of these energy levels:

$$\mathcal{P}(\epsilon_i) = \frac{1}{\sqrt{2\pi}\Delta} \exp\left(-\frac{\epsilon_i^2}{2\Delta^2}\right). \quad (2)$$

The parameter Δ represents the measure of disorder and this Gaussian random field (with “white noise” correlation on different lattice sites) generates “impurity” scattering and leads to the standard diagram technique for calculating the ensemble-averaged Green’s functions [26].

The generalized DMFT+ Σ approach [14–17] extends the standard DMFT [5–7] by introducing an additional self-energy $\Sigma_{\mathbf{p}}(\epsilon)$ (in the general case, momentum dependent), which is due to some interaction mechanism outside the DMFT. It gives an effective procedure to calculate both single- and two-particle properties [18, 21]. The single-particle Green’s function is then written in the form

$$G(\epsilon, \mathbf{p}) = \frac{1}{\epsilon + \mu - \epsilon(\mathbf{p}) - \Sigma(\epsilon) - \Sigma_{\mathbf{p}}(\epsilon)}, \quad (3)$$

where $\epsilon(\mathbf{p})$ is the “bare” electronic dispersion, while the total self-energy completely neglects the interference between the Hubbard and additional interaction and is given by the additive sum of the local self-energy $\Sigma(\epsilon)$ of DMFT and the “external” self-energy $\Sigma_{\mathbf{p}}(\epsilon)$. This preserves the standard structure of DMFT equations [5–7]. However, there are two important differences for the standard DMFT. At each iteration of the DMFT loop, we recalculate the “external” self-energy $\Sigma_{\mathbf{p}}(\epsilon)$ using some approximate scheme for the description of the “external” interaction, and the local Green’s function is “dressed” by $\Sigma_{\mathbf{p}}(\epsilon)$ at each step of the standard DMFT procedure.

In Fig. 1, we show the typical “skeleton” diagrams for self-energy in DMFT+ Σ . Here, the first two terms are local DFMT self-energy diagrams due to the Hubbard interaction, while two diagrams in the middle show contributions to self-energy from the additional interaction (dashed interaction lines), and the last diagram b is a typical example of the interference process,

which is neglected. Indeed, once we neglect such an interference, the total self-energy is defined as a simple sum of two contributions shown in Fig. 1a.

As an effective Anderson impurity solver in our DMFT calculations, we have always used the numerical renormalization group [27], which allows performing calculations at rather low temperatures.

For the self-energy due to disorder scattering produced by Hamiltonian (1), we use the simplest approximation neglecting the diagrams with “intersecting” interaction lines (like those in the fourth diagram in Fig. 1a), i. e., the so-called self-consistent Born approximation, represented by the third diagram in Fig. 1a. For the Gaussian distribution of site energies, it is momentum independent and is given by

$$\Sigma_{\mathbf{p}}(\varepsilon) \rightarrow \Delta^2 \sum_{\mathbf{p}} G(\varepsilon, \mathbf{p}), \quad (4)$$

where $G(\varepsilon, \mathbf{p})$ is the single-particle Green’s function (3), and Δ is the strength of site energy disorder.

In what follows, we mainly consider the three-dimensional system with a “bare” semi-elliptic density of states (per unit cell and one spin projection), with the total bandwidth $2D$, which is given by

$$N_0(\varepsilon) = \frac{2}{\pi D^2} \sqrt{D^2 - \varepsilon^2}. \quad (5)$$

In this case, we can directly demonstrate, that the disorder influence on single-particle properties of the disordered Hubbard model (both repulsive and attractive) is completely described in the DMFT+ Σ approximation by effects of general band widening by disorder scattering. Actually, in the system of self-consistent DMFT+ Σ equations [15, 17, 18], both the “bare” band spectrum and disorder scattering enter only at the stage of calculations of the local Green’s function:

$$G_{ii} = \sum_{\mathbf{p}} G(\varepsilon, \mathbf{p}), \quad (6)$$

where the full Green’s function $G(\varepsilon, \mathbf{p})$ is determined by Eq. (3), while the self-energy due to disorder, in the self-consistent Born approximation, is given by Eq. (4). Then the local Green’s function takes the form

$$\begin{aligned} G_{ii} &= \int_{-D}^D d\varepsilon' \frac{N_0(\varepsilon')}{\varepsilon + \mu - \varepsilon' - \Sigma(\varepsilon) - \Delta^2 G_{ii}} = \\ &= \int_{-D}^D d\varepsilon' \frac{N_0(\varepsilon')}{E_t - \varepsilon'}, \quad (7) \end{aligned}$$

where we introduce

$$E_t = \varepsilon + \mu - \Sigma(\varepsilon) - \Delta^2 G_{ii}.$$

In the case of a semi-elliptic density of states (5), this integral can be calculated in analytic form, and the local Green’s function then becomes

$$G_{ii} = 2 \frac{E_t - \sqrt{E_t^2 - D^2}}{D^2}. \quad (8)$$

It can be easily seen that Eq. (8) represents one of the roots of the quadratic equation

$$G_{ii}^{-1} = E_t - \frac{D^2}{4} G_{ii}, \quad (9)$$

reproducing the correct limit $G_{ii} \rightarrow E_t^{-1}$ for an infinitely narrow ($D \rightarrow 0$) band. Then we can write

$$\begin{aligned} G_{ii}^{-1} &= \varepsilon + \mu - \Sigma(\varepsilon) - \Delta^2 G_{ii} - \frac{D^2}{4} G_{ii} = \\ &= \varepsilon + \mu - \Sigma(\varepsilon) - \frac{D_{eff}^2}{4} G_{ii}, \quad (10) \end{aligned}$$

where we introduce the effective half-width of the band (in the absence of electronic correlations, i. e., for $U = 0$) widened by disorder scattering:

$$D_{eff} = D \sqrt{1 + 4 \frac{\Delta^2}{D^2}}. \quad (11)$$

Comparing (7), (9), and (10), we immediately see that the local Green’s function can be written as

$$G_{ii} = \int_{-D_{eff}}^{D_{eff}} d\varepsilon' \frac{\tilde{N}_0(\varepsilon')}{\varepsilon + \mu - \varepsilon' - \Sigma(\varepsilon)}, \quad (12)$$

where

$$\tilde{N}_0(\varepsilon) = \frac{2}{\pi D_{eff}^2} \sqrt{D_{eff}^2 - \varepsilon^2} \quad (13)$$

represents the density of states in the absence of the interaction U widened by disorder. The density of states in the presence of disorder remains semi-elliptic, and therefore all effects of disorder scattering on single-particle properties of the disordered Hubbard model in the DMFT+ Σ approximation reduce to only disorder widening of the conduction band, i. e., to the replacement $D \rightarrow D_{eff}$.

Within the DMFT+ Σ approach, we can also investigate the two-particle properties [18, 21]. After the general analysis based on the Ward identity derived in Ref. [21], we can show that the real part of the dynamical (optical) conductivity in the DMFT+ Σ approximation is given by [18, 21]

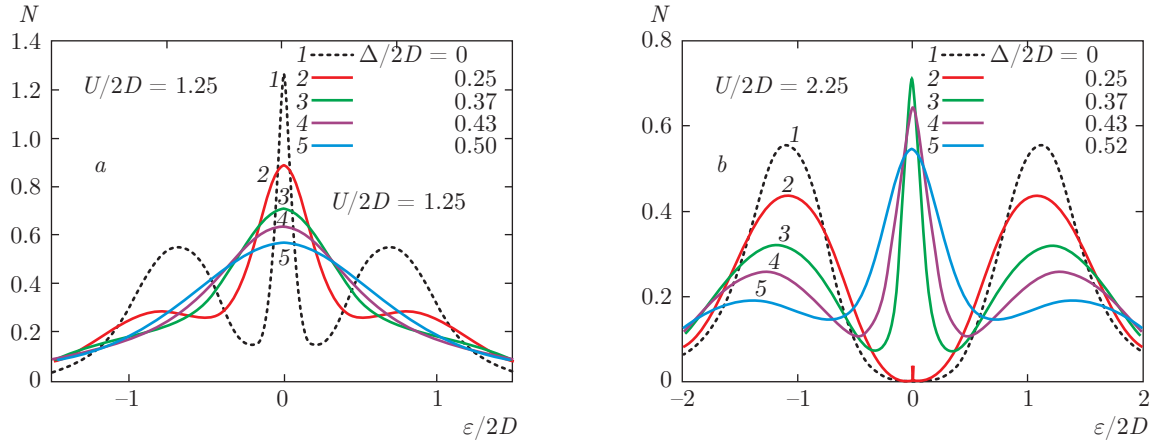


Fig. 2. Density of states of the Hubbard model at half-filling for different disorder levels Δ [18]. (a) Correlated metal with $U = 2.5D$. (b) Mott insulator with $U = 4.5D$. Temperature $T/2D = 0.0005$

$$\begin{aligned} \text{Re } \sigma(\omega) &= \frac{e^2 \omega}{2\pi} \int_{-\infty}^{\infty} d\varepsilon [f(\varepsilon_-) - f(\varepsilon_+)] \times \\ &\times \text{Re} \left\{ \phi_{\varepsilon}^{0RA}(\omega) \left[1 - \frac{\Sigma^R(\varepsilon_+) - \Sigma^A(\varepsilon_-)}{\omega} \right]^2 - \right. \\ &\left. - \phi_{\varepsilon}^{0RR}(\omega) \left[1 - \frac{\Sigma^R(\varepsilon_+) - \Sigma^R(\varepsilon_-)}{\omega} \right]^2 \right\}, \quad (14) \end{aligned}$$

where e is the electron charge, $f(\varepsilon_{\pm})$ is the Fermi distribution with $\varepsilon_{\pm} = \varepsilon \pm \omega/2$, and

$$\begin{aligned} \phi_{\varepsilon}^{0RR(RA)}(\omega) &= \\ &= \lim_{q \rightarrow 0} q^{-2} \left(\Phi_{\varepsilon}^{0RR(RA)}(\omega, \mathbf{q}) - \Phi_{\varepsilon}^{0RR(RA)}(\omega, 0) \right), \quad (15) \end{aligned}$$

where the two-particle loops $\Phi_{\varepsilon}^{0RR(RA)}(\omega, \mathbf{q})$ contain all vertex corrections from disorder scattering, but do not include any vertex corrections from Hubbard interaction (see the details in Ref. [18]). This considerably simplifies calculations of optical conductivity within the DMFT+ Σ approximation, because we only have to solve the single-particle problem for the local self-energy $\Sigma(\varepsilon_{\pm})$ via the DMFT+ Σ procedure, while nontrivial contributions from disorder scattering enter only via $\Phi_{\varepsilon}^{0RR(RA)}(\omega, \mathbf{q})$, which can be calculated in an appropriate approximation, neglecting vertex corrections from Hubbard interaction. To be more specific, to obtain the loop contributions $\Phi_{\varepsilon}^{0RR(RA)}(\omega, \mathbf{q})$ determined by disorder scattering, we can either use the standard “ladder” approximation for weak disorder or, following Ref. [18], use a direct generalization of the self-consistent theory of localization [28–30], which allows treating the case of strong enough disorder. In this ap-

proach, conductivity is mainly determined by the generalized diffusion coefficient obtained from a simple extension of the self-consistency equation [28–30] of this theory, which is to be solved in combination with the DMFT+ Σ procedure [18].

3. MOTT-ANDERSON TRANSITION IN DISORDERED SYSTEMS

Below, we present some of the most interesting results for the repulsive Hubbard model at half-filling with semi-elliptic bare density of states (5) with the bandwidth $2D$ [18], which is qualitatively well suited to describe the three-dimensional case. The density of states is given below in units of the number of states in the energy interval for a cubic unit cell of the volume a^3 (where a is the lattice constant) and for one spin projection. The conductivity values are always given in natural units of $e^2/\hbar a$.

3.1. Evolution of the density of states

In the standard DMFT approximation, the density of states of the repulsive Hubbard model at half-filling has a typical three-peak structure [5, 6, 32] with quite a narrow quasiparticle (central) peak at the Fermi level and rather wide upper and lower Hubbard bands located at energies $\varepsilon \sim \pm U/2$. As the Hubbard repulsive interaction U grows, the quasiparticle band narrows within the metallic phase and disappears at the Mott–Hubbard metal–insulator transition at the critical interaction value $U_{c2}/2D \approx 1.5$. At larger values of U , we observe an insulating gap at the Fermi level.

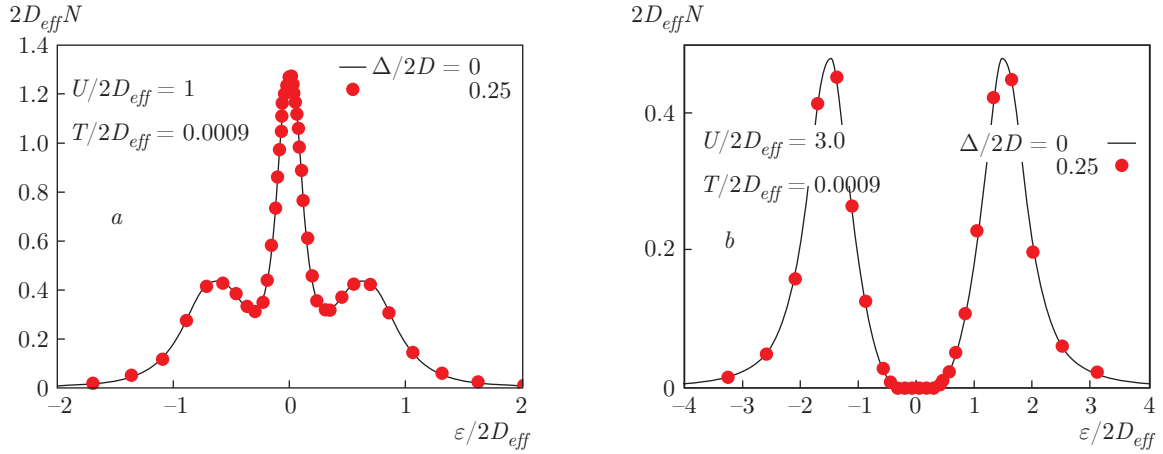


Fig. 3. Universal dependence of the properly normalized density of states on the normalized energy $\varepsilon/2D_{eff}$ in the Hubbard model for different disorder levels Δ . (a) correlated metal ($U/2D_{eff} = 1.0$) with no disorder and for $\Delta/2D = 0.25$. (b) Mott insulator ($U/2D_{eff} = 3.0$) without disorder and for $\Delta/2D = 0.25$. Temperature $T/2D_{eff} = 0.0009$

In Fig. 2, we present our results [18] for DMFT+ Σ densities of states for a typical strongly correlated metal with $U = 2.5D$, both in the absence of disorder and for different values of disorder scattering Δ , including strong enough disorder, which transforms the correlated metal to a correlated Anderson insulator. In the metallic phase, disorder scattering leads to a typical broadening and suppression of the density of states.

Much more unusual is the result obtained for $U = 4.5D$, typical for the Mott insulator phase and shown in Fig. 2b. Here, we observe the recovery of the central peak (quasiparticle band) in the density of states with an increase in disorder, transforming the Mott insulator to correlated metal or to a correlated Anderson insulator. A similar behavior of the density of states for the disordered Hubbard model was also reported in Ref. [31], using direct numerical DMFT calculations in finite lattices.

The physical origin of this quite unexpected central peak restoration is evident. The control parameter of the metal–insulator transition in DMFT is the ratio of the Hubbard interaction U to the bare bandwidth $2D$. Introduction of disorder (in the absence of Hubbard interaction) leads to a new effective bandwidth $2D_{eff}$ (cf. (11)), which increases with disorder. This leads to diminishing values of the ratio $U/2D_{eff}$, which in its turn causes the restoration of the quasiparticle band.

Furthermore, in complete accordance with analytic arguments presented above, the behavior of the density of states in the disordered Hubbard model with semi-elliptic density of states actually demonstrates a universal dependence on disorder. This is clearly seen from

Fig. 3, where we show properly normalized typical densities of states $2D_{eff}N(\varepsilon)$ in the metallic phase (with the normalized interaction value $U/2D_{eff} = 1.0$) and the insulating phase (corresponding to $U/2D_{eff} = 3.0$) without disorder and for the typical value of disorder scattering $\Delta/2D = 0.25$. The densities of states in the absence and in the presence of disorder are actually described by the same (universal) dependences if expressed via properly normalized parameters.

In the absence of disorder, one of the characteristic features of the Mott–Hubbard metal–insulator transition is the hysteresis behavior of the density of states, occurring as U decreases starting from the insulating phase [6, 32]. The Mott insulator phase remains (meta)stable down to rather small values of U deep within the correlated metal phase, and the metallic phase is restored only at about $U_{c1}/2D \approx 1$. The corresponding interval of the interaction parameter $U_{c1} < U < U_{c2}$ represents a coexistence region of the metallic and Mott insulating phases, where, from a thermodynamic standpoint, the metallic phase is more stable [6, 32, 33]. Such a hysteresis in the behavior of the density of states is also observed in the presence of disorder [18, 19].

3.2. Optical conductivity: Mott–Hubbard and Anderson transitions

In the absence of disorder, our calculations reproduce the conventional DMFT results [5, 6], with the optical conductivity characterized by a typical Drude peak at low frequencies and a wide maximum at $\omega \sim U$, which corresponds to optical transitions to the upper

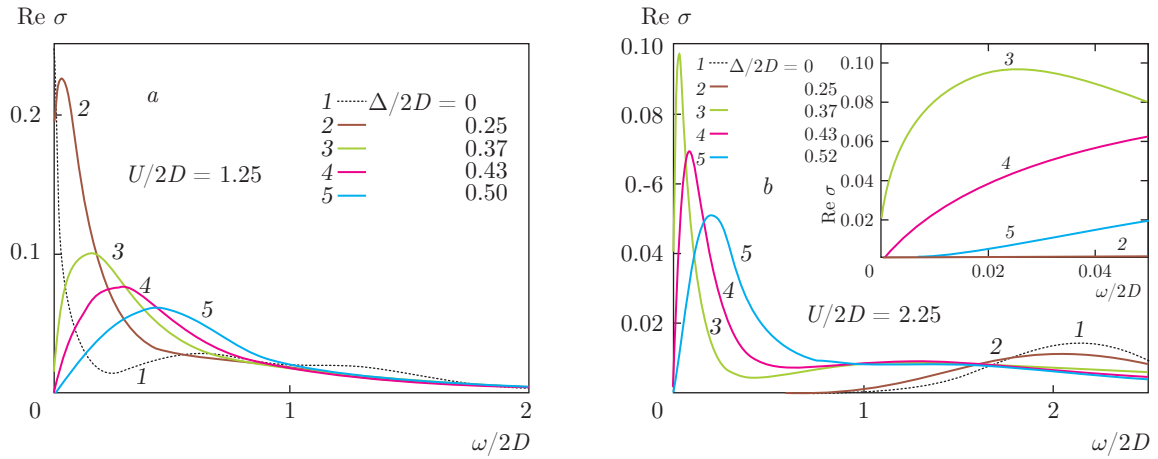


Fig. 4. Real part of the optical conductivity of the Hubbard model at half-filling for different disorder levels Δ [18]. (a) typical correlated metal with $U = 2.5D$. Curves 1, 2 describe the metallic phase, curve 3 corresponds to the mobility edge (Anderson transition), curves 4, 5 correspond to a correlated Anderson insulator. (b) typical Mott insulator with $U = 4.5D$. Curves 1, 2 correspond to a Mott insulator, curve 3 to the mobility edge (Anderson transition), curves 4, 5 to a correlated Anderson insulator. The inset shows the low-frequency region magnified. Temperature $T/2D = 0.0005$

Hubbard band. As U increases, the Drude peak is suppressed and disappears completely at the Mott transition. Introducing disorder leads to qualitative changes in the frequency dependence of the optical conductivity.

Figure 4a shows the real part of the optical conductivity of the Hubbard model at half-filling for different disorder levels Δ and $U = 2.5D$ typical for a correlated metal. Transitions to the upper Hubbard bands at energies $\omega \sim U$ are almost unobservable. However, it is clearly visible that the metallic Drude peak typically centered at the zero frequency is broadened and suppressed by disorder, gradually transforming into a peak at a finite frequency because of the Anderson localization effects. The Anderson transition takes place at $\Delta_c \approx 0.74D$ (corresponding to curve 3 on all figures here). We note that this value explicitly depends on the value of the cutoff in the equation for the generalized diffusion coefficient, which is defined up to a coefficient of the order of unity [26, 29]. Naive expectations can lead to the conclusion that a narrow quasiparticle band at the Fermi level (formed in a strongly correlated metal) can be localized much more easily than the usual conduction band. However, these expectations are wrong and the band localizes only at rather large disorder $\Delta_c \sim D$ of the order of the conduction band width $\sim 2D$. This is in qualitative agreement with the results for localization transition in the two-band model [36].

In the DMFT+ Σ approach, the critical disorder value Δ_c does not depend on U because the interaction effects enter here only through $\Delta\Sigma^{RA}(\omega) \rightarrow 0$ as $\omega \rightarrow 0$ (for $T = 0, \varepsilon = 0$), and therefore the influence of interaction just disappears at $\omega = 0$. In fact, this is the main shortcoming of the DMFT+ Σ approach, originating from the neglect of the interference effect between interaction and impurity scattering. A significant role of these interference effects is actually well known for a long time [34, 35]. However, the neglect of these effects allows us to perform a reasonable physical interpolation between two main limits: that of the Anderson transition due to disorder and the Mott–Hubbard transition due to strong correlations.

In Fig. 4b, we show the real part of the optical conductivity of the Mott–Hubbard insulator with $U = 4.5D$ for different disorder levels Δ . In the inset, we show low-frequency data, demonstrating different types of conductivity behavior, especially close to the Anderson transition and within the Mott insulator phase. On the main part of the figure, the contribution to conductivity from transitions to the upper Hubbard band at $\omega \sim U$ is clearly seen. Disorder growth results in the appearance of finite conductivity for the frequencies inside the Mott–Hubbard gap, correlating with the restoration of the quasiparticle band in the density of states within the gap as shown in Fig. 2b. This conductivity for $\Delta < \Delta_c$ is metallic (finite in the static limit $\omega = 0$), and for $\Delta > \Delta_c$ at low frequencies, we

obtain $\text{Re } \sigma(\omega) \sim \omega^2$, which is typical for an Anderson insulator [26, 28–30].

Somewhat unusual is the appearance in $\text{Re } \sigma(\omega)$ of a peak at finite frequencies even in the metallic phase. This happens because of the importance of localization effects. In the “ladder” approximation for $\Phi_\varepsilon^{0RA}(\omega, \mathbf{q})$, with all localization effects neglected, we obtain the usual Drude peak at $\omega = 0$ [18], while taking localization effects into account shifts the peak in $\text{Re } \sigma(\omega)$ to finite frequencies.

Above, we presented the data for conductivity obtained in the case of increasing U from the metallic to the Mott insulator phase. As U decreases from the Mott insulator phase, we observe a hysteresis of conductivity in the coexistence region defined (in the absence of disorder) by the inequality $U_{c1} < U < U_{c2}$. A hysteresis of conductivity is also observed in the coexistence region in the presence of disorder. More details can be found in Refs. [18, 19].

In general, the picture of the conductivity behavior obtained in the DMFT+ Σ approximation is rather rich, demonstrating both the Mott–Hubbard transition due to strong correlations and the disorder-induced Anderson (localization) transition. The complicated behavior under disordering is essentially determined by the two-particle Green’s function behavior and does not show a kind of universality demonstrated above for the single-particle density of states.

3.3. Phase diagram of the disordered Hubbard model at half-filling

The phase diagram of the repulsive disordered Hubbard model at half-filling was studied in Ref. [31], using direct DMFT numerics for lattices with a finite number of sites with random realizations of energies ε_i in (1), with subsequent averaging over many lattice realizations to obtain the averaged density of states and the geometric mean local density of states, which allows determining the critical disorder for the Anderson transition. Below, we present our results on the disordered Hubbard-model phase diagram obtained from the density of states and optical conductivity calculations in the DMFT+ Σ approach [18].

The calculated disorder–correlation strength (Δ, U) phase diagram at zero temperature is shown in Fig. 5 (actual calculations were performed at a very low value $T/2D = 0.0005$). The Anderson transition line $\Delta_c \approx 0.37D$ is defined as the disorder strength for which static conductivity vanishes at $T = 0$. The Mott–Hubbard transition can be detected either from the cen-

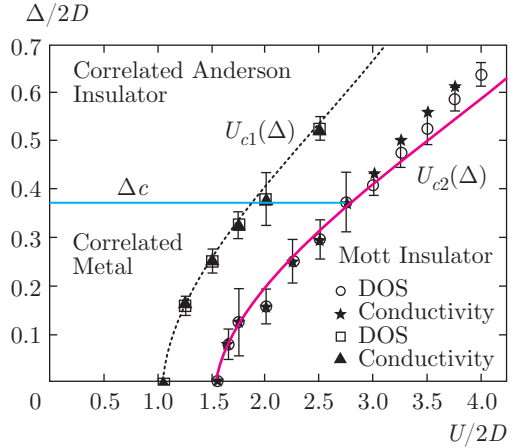


Fig. 5. Phase diagram of the disordered Hubbard model [18]. Continuous curves are Mott insulator phase boundaries $U_{c1,c2}(\Delta)$ obtained from the analytic estimate in Eq. (17). Different symbols represent results for these boundaries obtained from calculations from the density of states and optical conductivity. The Anderson transition line is given by $\Delta_c = 0.37$

tral peak disappearance in the density of states or from the optical conductivity by observation of gap closing in the insulating phase or from the static conductivity disappearance in the metallic phase.

We have already noted that the DMFT+ Σ approximation gives a universal (U -independent) value of the critical disorder Δ_c because of the neglect of interference between disorder scattering and Hubbard interaction. This leads to a difference between the phase diagram in Fig. 5 and the one obtained by numerical simulations in Ref. [31]. At the same time, the qualitative form of our phase diagram is highly nontrivial and qualitatively coincides with the results in Ref. [31]. The main difference is the conservation of Hubbard bands in our results even in the limit of high enough disorder, while they just disappear in Ref. [31]. The phase coexistence region in Fig. 5 slowly widens as disorder increases instead of vanishing at some “critical” point as on the phase diagram in Ref. [31]. The coexistence boundaries (Mott insulator phase boundaries) obtained with a decrease or increase in U , represented by curves $U_{c1}(\Delta)$ and $U_{c2}(\Delta)$ in Fig. 5, can actually be obtained from the simple equation

$$\frac{U_{c1,c2}(\Delta)}{D_{eff}} = \frac{U_{c1,c2}}{D}, \quad (16)$$

where the effective bandwidth in the presence of disorder is calculated for $U = 0$ within self-consistent Born approximation (4), (11). Hence, the boundaries of the

coexistence region (which also define the boundaries of the Mott insulator phase) are given by

$$U_{c1,c2}(\Delta) = U_{c1,c2} \sqrt{1 + 4 \frac{\Delta^2}{D^2}}. \quad (17)$$

They are shown in Fig. 5 by dotted and solid lines. Phase transition points detected from the disappearance of a quasiparticle peak as well as points following from qualitative changes of conductivity behavior are shown in Fig. 5 by different symbols. These symbols demonstrate very good agreement with analytic results, confirming the choice of ratio (16) as a control parameter of the Mott transition in the presence of disorder. This transition is essentially controlled by simple band-widening effects due to disorder scattering, similarly to the behavior of the density of states discussed above.

We note that the values of the normalized density of states $2D_{eff}N(\varepsilon)$ are universal along each of these boundaries, as well as along any curve in the (Δ, U) plane determined by the equation

$$U(\Delta) = U(0) \sqrt{1 + 4 \frac{\Delta^2}{D^2}} \quad (18)$$

in accordance with our discussion of the universal dependence of the densities of states on disorder presented above.

Essentially similar results were obtained for the behavior of the density of states, dynamic conductivity, and the phase diagram [19] in the case of the conduction band with a “flat” density of states in the absence of disorder and interactions, which qualitatively corresponds to the two-dimensional case. This is not surprising because large enough disorder and interactions both transform the “flat” band into a kind of smeared semi-elliptic band. Some explicit examples of this kind of behavior are presented below in the case of the attractive Hubbard model.

4. ATTRACTIVE HUBBARD MODEL WITH DISORDER

The studies of superconductivity in the BCS–BEC crossover region attracts theorists for a rather long time [10] and most important progress here was achieved by Nozieres and Schmitt-Rink [11], who proposed an effective approach to describe the T_c crossover. The attractive Hubbard model is probably the simplest model allowing theoretical studies of the BCS–BEC crossover [11]. This model was studied within DMFT in a number of recent papers [37–40]. But only a few results were

obtained for the normal (nonsuperconducting) phase of this model, especially in the disordered case. Similarly, there were practically no studies of two-particle properties, such as optical conductivity. Below, we present a summary of our results obtained within the DMFT+ Σ approach and compare then with similar results for the repulsive Hubbard model.

4.1. Density of states and optical conductivity

In the special case of a half-filled band ($n = 1$), the densities of states of attractive and repulsive Hubbard models just coincide (due to an exact mapping of these models onto each other). Below, we discuss the more typical case of a quarter-filled band ($n = 0.5$). In Fig. 6, we show the densities of states obtained for $T/2D = 0.05$ for different values of attractive interaction ($U < 0$). Figure 6a is to be compared with Fig. 6b, where we present similar results for the repulsive ($U > 0$) case. We can see that the densities of states close to the Fermi level decrease with an increase in U , both for attraction (Fig. 6a) and repulsion (Fig. 6b), but a significant increase in $|U|$ in the repulsive case leads only to the vanishing of the quasiparticle peak, such that the density of states at the Fermi level becomes practically independent of U , while in the attractive case, the increase in $|U|$ leads to the superconducting pseudogap opening at the Fermi level (curve 3 in Fig. 6a); for $|U|/2D > 1.2$, we observe the full gap opening at the Fermi level (curves 4, 5 in Fig. 7). This gap is not directly related to the emergence of a superconducting state, but is due to the appearance of preformed Cooper pairs at the temperatures larger than the superconducting transition temperature (which is lower than the temperature $T/2D = 0.05$ used in our calculations). Here, we actually observe the important difference between attractive and repulsive cases: in case of repulsion, a deviation from half-filling leads to a metallic state for arbitrary values of U and the insulating gap opens at large U not at the Fermi level.

This picture of the evolution of the density of states as $|U|$ increases is also supported by the behavior of optical conductivity shown in Fig. 7. We see that the increase in $|U|$ leads to the replacement of the Drude peak at zero frequency (curves 1–3 in Fig. 7) by a pseudogap dip (curves 5 and 6 in Fig. 7) and a wide maximum of the conductivity at a finite frequency, related with transitions across the pseudogap. A further increase in $|U|$ leads to the opening of the full gap in the optical conductivity due to the formation of Cooper pairs (curves 7–9 in Fig. 7).

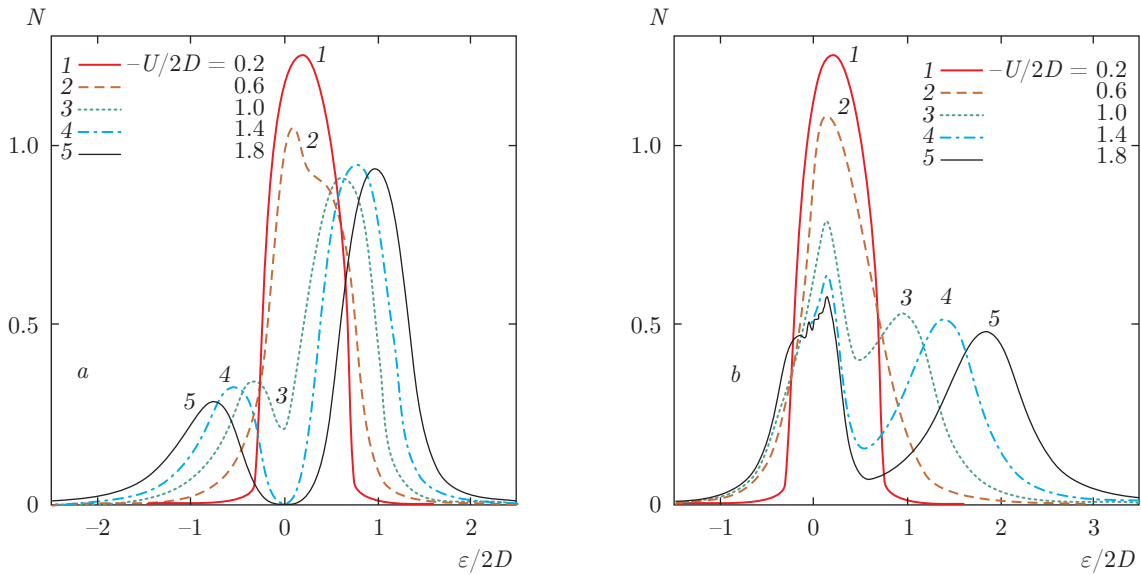


Fig. 6. Densities of states for different values of Hubbard (a) attraction and (b) repulsion. Temperature $T/2D = 0.05$

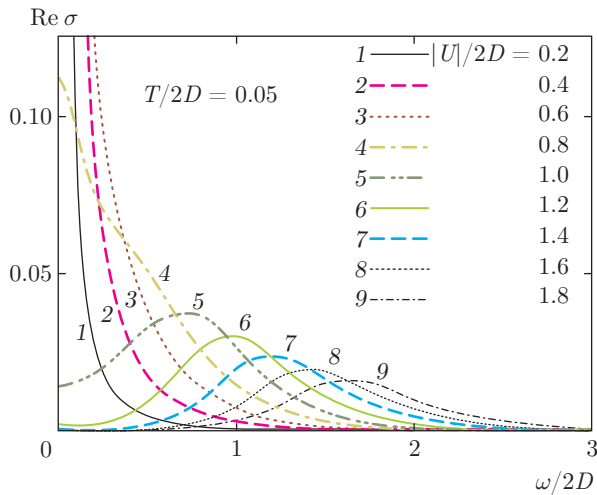


Fig. 7. Optical conductivity for different values of attractive Hubbard model. Temperature $T/2D = 0.05$

In Fig. 8, we present the evolution of the density of states and optical conductivity with changing disorder. At weak enough attraction ($|U|/2D = 0.8$, Fig. 8a,b), the growth of disorder just widens the density of states. Disorder effectively masks peculiarities of the density of states due to correlation effects. In particular, the quasiparticle peak and the “wings” due to the upper and lower Hubbard bands presented in Fig. 8a in the absence of disorder completely vanish at strong enough disorder. Evolution of the optical conductivity with the growth of disorder Δ , shown in

Fig. 8b, generally agrees with the evolution of the density of states. Weak enough disorder (curves 1, 2 in Fig. 8b) leads to some increase in the static conductivity, which is related with suppression of correlation effects at the Fermi level (curves 1, 2 in Fig. 8a). Further increasing disorder leads to significant widening of the band and a decrease in the density of states (curve 3 in Fig. 8a,b), which leads to a decrease in static conductivity. Finally, the growth of disorder leads to Anderson localization, which occurs at $\Delta/2D = 0.37$ for $T = 0$ [18]. However, we here consider the case of a sufficiently high temperature $T/2D = 0.05$, such that the static conductivity (see curve 5 in Fig. 8b) always remains finite, although the localization behavior is also clearly seen and $\sigma(\omega) \sim \omega^2$. At larger values of the attractive interaction $|U|/2D = 1$, the evolution of the density of states and optical conductivity are largely similar (Fig. 8c,d). But in the absence of disorder, we then observe a Cooper pairing pseudogap in the density of states, while disorder leads to its suppression, leading both to the growth of the density of states at the Fermi level and the related growth of static conductivity. Finally, at a still larger attraction $|U|/2D = 1.6$ (Fig. 8e,f) in the absence of disorder, there is a real Cooper pairing gap in the density of states. This gap is also evident in the optical conductivity. With an increase in disorder, the Cooper pairing gap in both the density of states and conductivity becomes narrower (curves 2, 3). A further increase in disorder leads to the complete suppression of this gap and restoration of a metallic state with a finite density of states at the

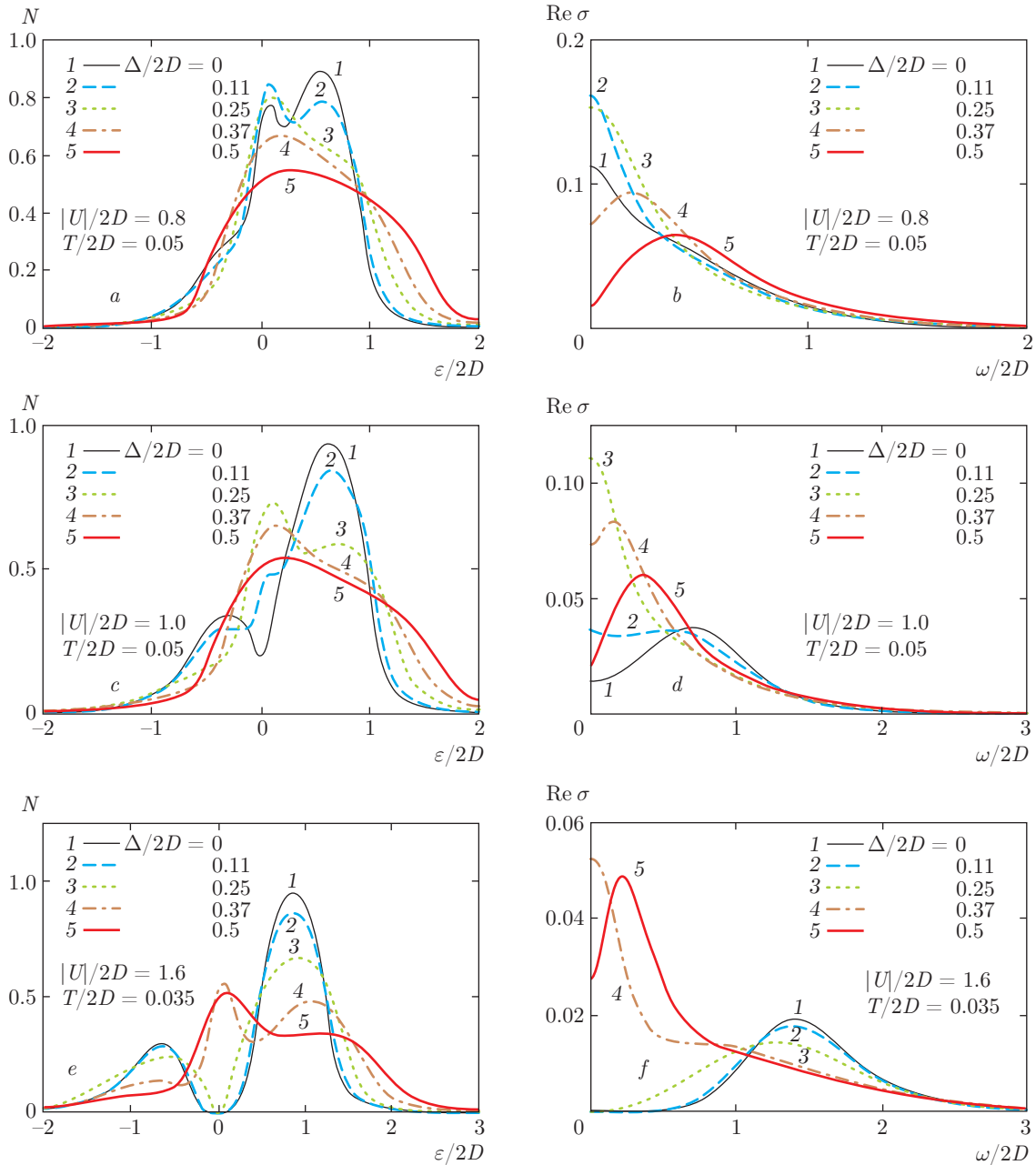


Fig. 8. Evolution of the density of states (left panels) and optical conductivity (right panels) with disorder for different values of U ((a),(b): $|U|/2D = 0.8$, (c),(d): $|U|/2D = 1$, (e),(f): $|U|/2D = 1.6$)

Fermi level and finite static conductivity. This closure of the Cooper gap is obviously related to the effective growth of the conduction bandwidth $2D_{eff}$, which leads to the decrease in the $|U|/2D_{eff}$ ratio, which actually controls the formation of the Cooper gap. The situation here is similar to the closure of the Mott gap by disorder in the repulsive Hubbard model discussed above [18]. However, at large disorder (curve 5 in Fig. 8f),

we clearly observe the localization behavior, such that the growth of disorder at $T = 0$ first leads to a metallic state (the closure of the Cooper pairing gap), while the further growth induces the Anderson metal–insulator transition. A similar picture is observed for large positive U at half-filling ($n = 1$) [18], where the growth of disorder leads to the Mott-insulator–correlated-metal–Anderson-insulator transition.

We now demonstrate the universality of the disorder dependence of the density of states as an example of the most important single-particle property. We concentrate on the most typical case of the evolution of the density of states shown in Fig. 8*a*. We can easily convince ourselves that this evolution is only due to the general widening of the band due to disorder (cf. (11)), because all the data for the density of states fit the same universal curve replotted in appropriate new variables, with all energies (and temperature) normalized by the effective bandwidth by replacing $D \rightarrow D_{eff}$, as shown in Fig. 9*a*, in complete accordance with results obtained above in the repulsive Hubbard model for a semi-elliptic band.

In the case of the initial (“bare”) conduction band with a flat density of states, there is no complete universality, as is seen from Fig. 9*b* for sufficiently low values of disorder. However, for large disorder, the dashed curve in Fig. 9*b* practically coincides with universal curve for the density of states shown in Fig. 9*a*. This reflects the simple fact that at enough disorder, the flat density of states is effectively transformed into a semi-elliptic one [24].

4.2. Generalized Anderson theorem

The superconducting transition temperature T_c is not a single-particle characteristic of the system in general. The Cooper instability determining T_c is related to a divergence of the two-particle loop in the Cooper channel. In the weak-coupling limit, when superconductivity is due to the appearance of Cooper pairs at T_c , disorder only slightly influences superconductivity with *s*-wave pairing [41, 42]. This is the essence of the so-called Anderson theorem, and changes of T_c are only due to the relatively small changes of the density of states at the Fermi level induced by disorder.

In the BCS–BEC crossover region and in the strong-coupling region, the Nozieres–Schmitt-Rink approach [11] assumes that corrections due to strong pairing attraction significantly change the chemical potential of the system, while possible corrections due to this interaction to the Cooper instability condition can be neglected, and we can hence always use the weak-coupling (ladder) approximation. Then the condition of a Cooper instability in the disordered Hubbard model takes the form

$$1 = -|U|\chi_0(q = 0, \omega_m = 0), \tag{19}$$

where

$$\chi_0(q = 0, \omega_m = 0) = -T \sum_n \sum_{\mathbf{p}\mathbf{p}'} \Phi_{\mathbf{p}\mathbf{p}'}(\varepsilon_n) \tag{20}$$

represents the two-particle loop (susceptibility) in the Cooper channel “dressed” only by disorder scattering, and $\Phi_{\mathbf{p}\mathbf{p}'}(\varepsilon_n)$ is the averaged two-particle Green’s function in the Cooper channel ($\omega_m = 2\pi mT$ and $\varepsilon_n = \pi T(2n + 1)$ are the usual boson and fermion Matsubara frequencies).

Using the exact Ward identity derived in Ref. [21],

$$G(\varepsilon_n, \mathbf{p}) - G(-\varepsilon_n, -\mathbf{p}) = - \sum_{\mathbf{p}'} \Phi_{\mathbf{p}\mathbf{p}'}(\varepsilon_n) \times (G_0^{-1}(\varepsilon_n, \mathbf{p}') - G_0^{-1}(-\varepsilon_n, -\mathbf{p}')), \tag{21}$$

where $G(\varepsilon_n, \mathbf{p})$ is the impurity-averaged single-particle Green’s function (not containing Hubbard interaction corrections!), we can show [24] that Cooper susceptibility (20) is given by

$$\begin{aligned} \chi_0(q = 0, \omega_m = 0) &= \\ &= T \sum_n \frac{1}{2i\varepsilon_n} \left(\sum_{\mathbf{p}} G(\varepsilon_n, \mathbf{p}) - \sum_{\mathbf{p}} G(-\varepsilon_n, \mathbf{p}) \right) = \\ &= T \sum_n \frac{1}{i\varepsilon_n} \sum_{\mathbf{p}} G(\varepsilon_n, \mathbf{p}). \end{aligned} \tag{22}$$

After the standard summation over Matsubara frequencies [26], we obtain

$$\begin{aligned} \chi_0(q = 0, \omega_m = 0) &= \frac{1}{4\pi i} \times \\ &\times \int_{-\infty}^{\infty} \frac{d\varepsilon}{\varepsilon} \left(\sum_{\mathbf{p}} G^R(\varepsilon, \mathbf{p}) - \sum_{\mathbf{p}} G^A(\varepsilon, \mathbf{p}) \right) \text{th} \frac{\varepsilon}{2T} = \\ &= - \int_{-\infty}^{\infty} \frac{d\varepsilon}{2\varepsilon} \tilde{N}_0(\varepsilon) \text{th} \frac{\varepsilon}{2T}, \end{aligned} \tag{23}$$

where $\tilde{N}_0(\varepsilon)$ is the density of states ($U = 0$) renormalized by disorder scattering. In Eq. (23), the energy ε origin is at the chemical potential. If the origin of energy is shifted to the middle of the conduction band, we have to replace $\varepsilon \rightarrow \varepsilon - \mu$, and the condition of Cooper instability (19) leads to the following equation for T_c :

$$1 = \frac{|U|}{2} \int_{-\infty}^{\infty} d\varepsilon \tilde{N}_0(\varepsilon) (\varepsilon - \mu)^{-1} \text{th} \frac{\varepsilon - \mu}{2T_c}. \tag{24}$$

The chemical potential of the system at different values of U and Δ should now be determined from DMFT+ Σ calculations, i. e., from the standard equation for the number of electrons (band-filling), determined by the Green’s function given by Eq. (3), which allows finding T_c for a wide range of model parameters, including the BCS–BEC crossover and strong

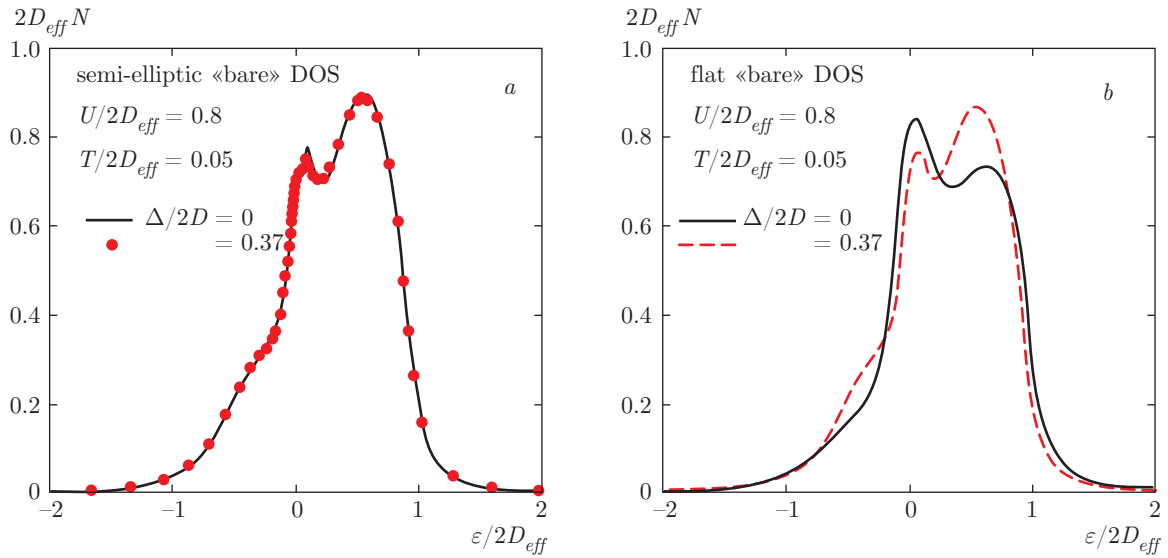


Fig. 9. Universal dependence of the density of states on disorder in the attractive Hubbard model: (a) the model of a semi-elliptic “bare” density of states, (b) the model of a flat “bare” density of states

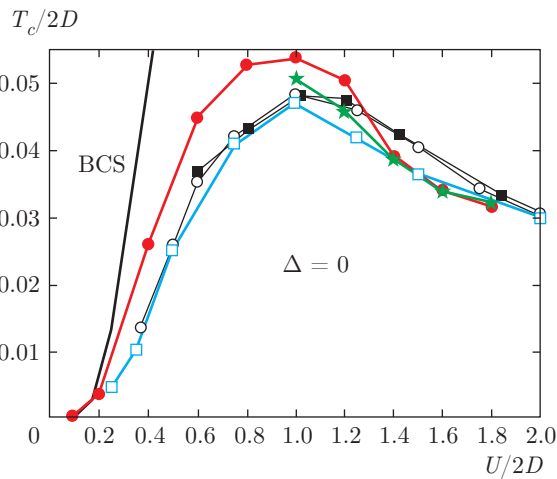


Fig. 10. Dependence of the superconducting critical temperature on the attractive interaction strength. Black squares, white circles, and white squares respectively show the results in Refs. [37, 38, 40] for a quarter-filled band with $n = 0.5$. Stars represent the results obtained numerically from the instability criterion for the normal phase in Ref. [22]. Filled circles show T_c in the Nozieres–Schmitt-Rink approximations, combined with DMFT [22]. The continuous black curve represents the BCS theory result

coupling regions, as well as for different levels of disorder. This is the gist of the Nozieres–Schmitt-Rink approximation: in the weak coupling region, the superconducting transition temperature is controlled by the equation for Cooper instability (24), while in the

strong-coupling limit, it is determined by the temperature of Bose–Einstein condensation, which is controlled by the chemical potential. Then the joint solution of Eq. (24) and the equation for the chemical potential guarantees the correct interpolation for T_c through the BCS–BEC crossover region. In the absence of disorder, this combination of the Nozieres–Schmitt-Rink approximation with DMFT produces the results for the critical temperature, which, as shown in Fig. 10, are almost quantitatively close to the exact results obtained by direct numerical DMFT calculations [22, 37, 38, 40], but demand much less numerical efforts.

Equation (24) demonstrates that the Cooper instability depends on disorder only through the disorder dependence of the density of states $\tilde{N}_0(\epsilon)$, which is the main statement of the Anderson theorem. Within the Nozieres–Schmitt-Rink approach, Eq. (24) is also preserved in the strong-coupling region, where the critical temperature is determined by the BEC condition for compact Cooper pairs. However, the chemical potential μ entering Eq. (24) may significantly depend on disorder. In the DMFT+ Σ approximation, this dependence of the chemical potential (as well as any other single-particle characteristics) in the model with a semi-elliptic density of states is only due to the disorder widening of the conduction band. In this sense, both in the BCS–BEC crossover region and in the strong-coupling limit, a kind of generalized Anderson theorem actually holds and Eq. (24) leads to a universal dependence of T_c on disorder, due to the change

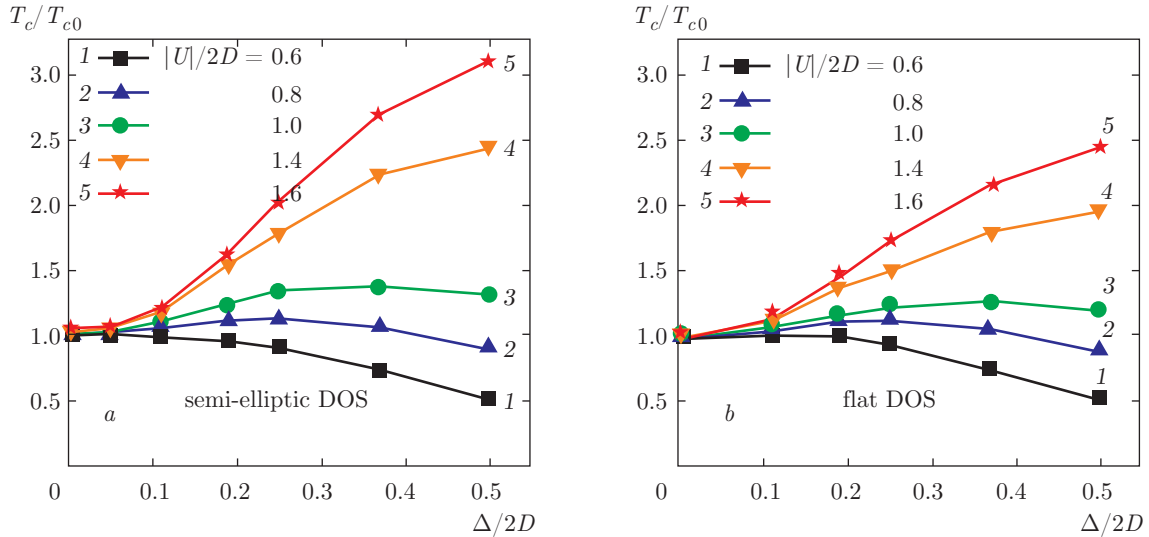


Fig. 11. Dependence of superconducting transition temperature on disorder for different values of Hubbard attraction U : (a) semi-elliptic band, (b) flat band

$D \rightarrow D_{eff}$. Such a universality is fully confirmed by direct numerical calculations of T_c in this model, performed in Ref. [23].

In Fig. 11, we present the dependence of T_c (normalized by the critical temperature in the absence of disorder $T_{c0} = T_c(\Delta = 0)$) on disorder for different values of the pairing interaction U for both models of the initial semi-elliptic density of states (Fig. 11a) and for a flat density of states (Fig. 11b). Qualitatively, the evolution of T_c with disorder is the same for both models. In the weak-coupling limit ($U/2D \ll 1$), disorder slightly suppresses T_c (curves 1). At intermediate couplings ($U/2D \sim 1$), weak disorder increases T_c , while a further increase in disorder suppresses the critical temperature (curves 3). In the strong-coupling region ($U/2D \gg 1$), the growth of disorder leads to a significant increase in the critical temperature (curves 4, 5). But this rather complicated dependence of T_c on disorder is actually completely determined simply by disorder widening of the initial ($U = 0$) conduction band, demonstrating the validity of the generalized Anderson theorem for all values of U . In Fig. 12, the curve with octagons shows the dependence of the critical temperature $T_c/2D$ on the coupling strength $U/2D$ in the absence of disorder ($\Delta = 0$) for both models of the initial conduction bands (semi-elliptic in Fig. 12a and flat in Fig. 12b). In both models, the superconducting transition temperature is well described by the BCS model in the weak-coupling region (in Fig. 12a, the dashed curve represents a solution of the BCS model, with T_c determined by Eq. (24), with the chemical potential

dependent of U and determined by the quarter-filling of the “bare” band), while in the strong-coupling region, the critical temperature is determined by Bose–Einstein condensation of Cooper pairs and decreases as t^2/U with an increase in U (inversely proportional to the effective mass of the pair), passing through a maximum at $U/2D_{eff} \sim 1$. The other symbols in Fig. 12a show the results for T_c obtained by a combination of the DMFT+ Σ and Nozieres–Schmitt-Rink approximations for a semi-elliptic band. We can see that all data (expressed in normalized units of $U/2D_{eff}$ and $T_c/2D_{eff}$) ideally fit the universal curve obtained in the absence of disorder. For a flat band, the results of our calculations are shown in Fig. 12b and we do not observe the complete universality: data points corresponding to different degrees of disorder slightly deviate from the curve obtained in the absence of disorder. However, with an increase in disorder, the flat density of states gradually transforms to a semi-elliptic one and our data points move toward the universal curve obtained in the semi-elliptic case and shown by the dashed curve in Fig. 12b, confirming the validity of the generalized Anderson theorem also in this case.

4.3. Ginzburg–Landau coefficients

The universal dependence on disorder is also observed for the Ginzburg–Landau expansion coefficients A (the homogeneous quadratic term of the expansion) and B (the fourth-order term), related to Cooper-channel vertices with the zero sum of incoming (out-

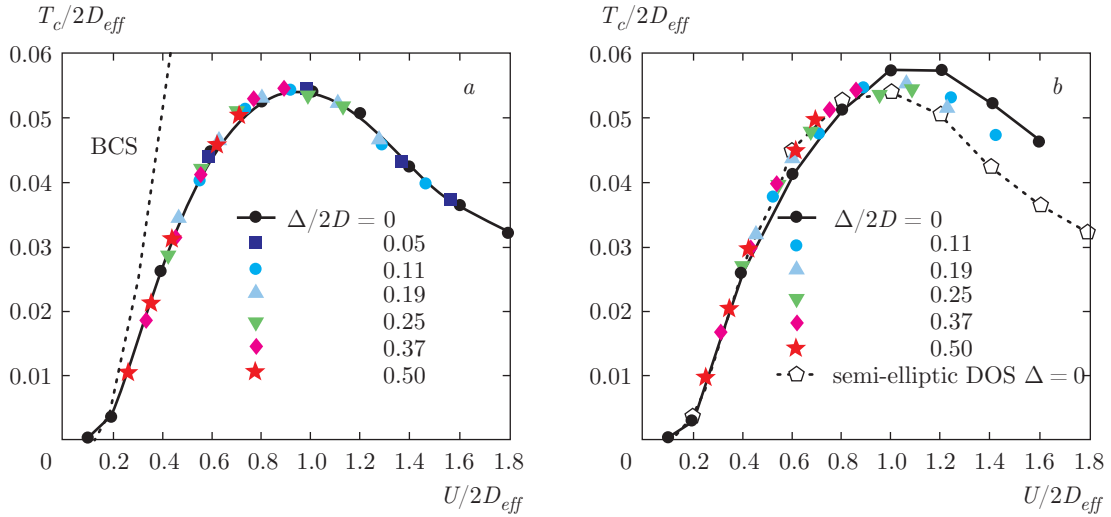


Fig. 12. Universal dependence of the superconducting critical temperature on the Hubbard attraction U for different disorder levels: (a) semi-elliptic band. The dashed curve represents the BCS dependence in the absence of disorder, (b) flat band. The dashed line represents a similar dependence for a semi-elliptic band at $\Delta = 0$

going) momenta, $q = 0$. The coefficient A is given by [26]

$$A(T) = \chi_0(q = 0, T) - \chi_0(q = 0, T_c), \quad (25)$$

where $\chi_0(q = 0, T)$ is Cooper susceptibility (20), and subtraction of $\chi_0(q = 0, T_c)$ guarantees the zero value of $A(T = T_c)$. Using (19) to determine $\chi_0(q = 0, T_c)$ and (23) for $\chi_0(q = 0, T)$, we obtain

$$A(T) = \frac{1}{|U|} - \int_{-\infty}^{\infty} d\varepsilon \tilde{N}_0(\varepsilon) (2(\varepsilon - \mu))^{-1} \text{th} \frac{\varepsilon - \mu}{2T}, \quad (26)$$

whence the coefficient $A(T)$ vanishes as $T \rightarrow T_c$, and can be written as

$$A(T) = a(T - T_c). \quad (27)$$

For a “bare” band with a semi-elliptic density of states, the dependence of a on disorder is related only to the general widening of the band by disorder, i. e., is completely described by the replacement $D \rightarrow D_{eff}$. Thus, in the presence of disorder, we obtain the universal dependence of a on U (normalized by D_{eff}), shown in Fig. 13a.

The Ginzburg–Landau coefficient B is determined by the “loop” diagram with four Cooper vertices [26]. After a rather complicated analysis, to be presented elsewhere, based on some generalizations of Ward identity (21), it can be shown exactly that B is given by

$$B = \int_{-\infty}^{\infty} \frac{d\varepsilon}{4(\varepsilon - \mu)^3} \times \left(\text{th} \frac{\varepsilon - \mu}{2T} - \frac{(\varepsilon - \mu)/2T}{\text{ch}^2(\varepsilon - \mu)/2T} \right) \tilde{N}_0(\varepsilon). \quad (28)$$

Hence, the dependence of the coefficient B on disorder, similarly to A , is determined only by the density of states $\tilde{N}_0(\varepsilon)$ renormalized (widened) by disorder and the chemical potential μ . Then, in the case of a semi-elliptic density of states, the dependence of B on disorder is reduced to the simple replacement $D \rightarrow D_{eff}$, and the presence of disorder we again obtain the universal dependence of B on U , shown in Fig. 13b.

We note that Eqs. (26) and (28) for the coefficients A and B were obtained using the exact Ward identities and also remain valid in the limit of strong disorder (the Anderson localized phase), where both A and B depend on disorder also only via the effective bandwidth D_{eff} .

This universal dependence on disorder (due to only the replacement $D \rightarrow D_{eff}$) is also reflected in the specific heat discontinuity at the transition temperature, which is determined by the coefficients a and B :

$$C_s(T_c) - C_n(T_c) = T_c \frac{a^2}{B}. \quad (29)$$

To determine the coefficient C in the gradient term of the Ginzburg–Landau expansion, we need the knowledge of the nontrivial q -dependence of the Cooper vertex [26], which is essentially changed by disorder scattering. In particular, the behavior of the coeffi-

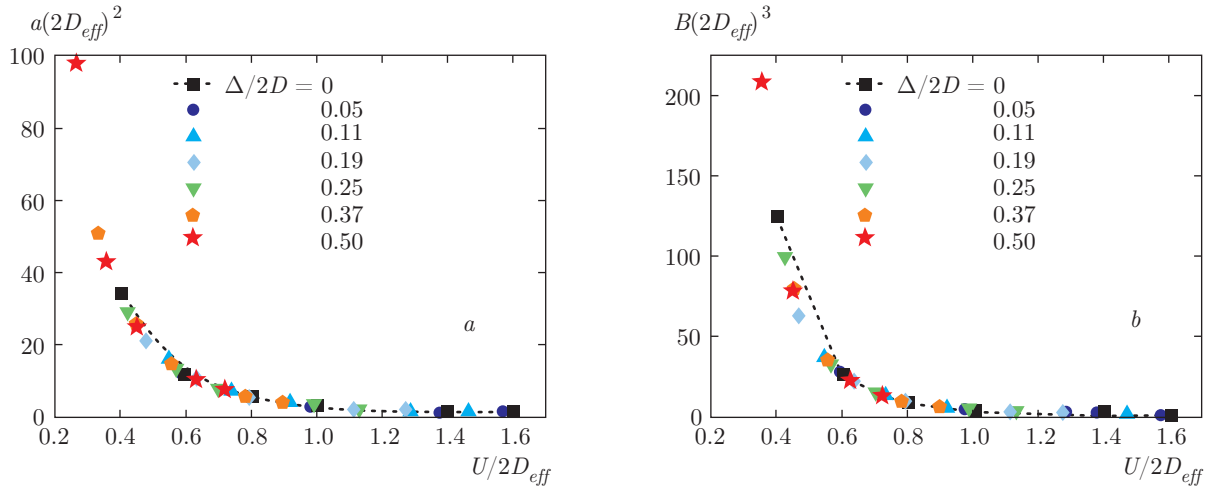


Fig. 13. Universal dependence of the Ginzburg–Landau coefficients (a) a and (b) B on the Hubbard attraction for different disorder levels. The dotted line with black squares shows the case $\Delta = 0$

cient C qualitatively changes at the Anderson localization transition [41]. Thus, the coefficient C is basically determined by two-particle characteristics of the system and does not demonstrate a universal dependence on disorder due to only changes of the effective bandwidth.

4.4. Number of local pairs

Disorder in the attractive Hubbard model also leads to the suppression of the number of local pairs (doubly occupied sites). The average number of local pairs is determined by the local (single site) pair correlation function $\langle n_{\uparrow}n_{\downarrow} \rangle$, which in the absence of disorder increases with the increase in the Hubbard attraction U from $\langle n_{\uparrow}n_{\downarrow} \rangle = \langle n_{\uparrow} \rangle \langle n_{\downarrow} \rangle = n^2/4$ for $U/2D_{eff} \ll 1$ to $\langle n_{\uparrow}n_{\downarrow} \rangle = n/2$ for $U/2D_{eff} \gg 1$, when all electrons become paired. In our calculations, $n = 0.5$ (a quarter-filled band), whence $n/2 = 0.25$ and $n^2/4 = 0.0625$. The increase in D_{eff} with disorder leads to an effective suppression of the parameter $U/2D_{eff}$ and the corresponding suppression of the number of doubly occupied sites. In Fig. 14a, we show the disorder dependence of the number of doubly occupied sites for three different values of the Hubbard attraction. In all cases, the growth of disorder suppresses the number of doubly occupied sites (local pairs). Similarly to T_c , the change of the number of local pairs with disorder can be attributed only to the change of the effective bandwidth (11) with the increase in disorder. In Fig. 14b, the curve with black squares shows the dependence of the number of doubly occupied sites on attractive interaction in the absence of disorder at the temperature

$T/2D = 0.0586$. This curve is actually universal: the dependence of the number of local pairs $\langle n_{\uparrow}n_{\downarrow} \rangle$ on the scaled parameter $U/2D_{eff}$ with an appropriately scaled temperature $T/2D_{eff} = 0.0586$ in the presence of disorder is given by the same curve that is shown by circles representing data obtained for five different disorder levels shown in Fig. 14b for $U/2D = 1$.

5. CONCLUSION

In this paper, in the framework of the DMFT+ Σ generalization of dynamic mean field theory [17], we have studied and compared disorder effects in both repulsive and attractive Hubbard models. We examined the problems of both Mott–Hubbard and Anderson–metal–insulator transitions in repulsive case, and the BCS–BEC crossover region of the attractive Hubbard model. We also performed extensive calculations of the densities of states and dynamic (optical) conductivity for a wide range of interactions U and at different disorder levels Δ , demonstrating similarities and dissimilarities between repulsive and attractive cases.

We have shown analytically for case conduction band with a semi-elliptic density of states (which is a good approximation for the three-dimensional case) that in the DMFT+ Σ approximation, disorder influences all single-particle properties (e.g., density of states) in a universal way: all changes of these properties are due to only the disorder widening of the conduction band. In the model of a conduction band with a flat density of states (which is more appropriate for two-dimensional systems), there is no such

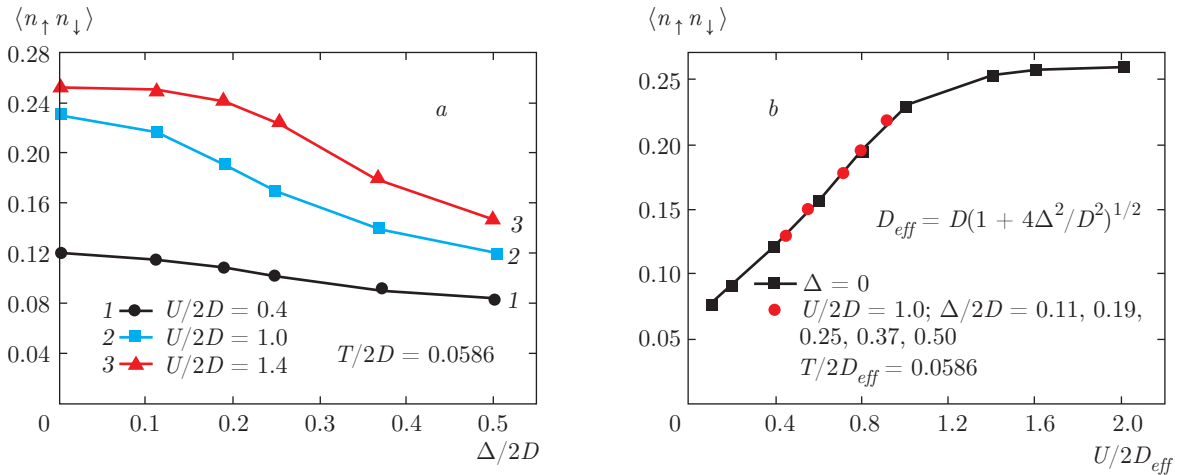


Fig. 14. (a) Dependence of the number of local pairs on disorder for different values of the Hubbard attraction and (b) the universal dependence on disorder expressed via normalized variables at the fixed value $U/2D = 1$

an universality in the region of weak disorder. But the main effects are again due to the general widening of the band and the complete universality is restored for high enough disorder, when the density of states effectively becomes semi-elliptic. Similar universal dependences on disorder are also reflected in the phase diagram of the repulsive Hubbard model and in the superconducting critical temperature of the attractive Hubbard model, where the combination of DMFT+ Σ and Nozieres–Schmitt-Rink approximations demonstrates the validity of the generalized Anderson theorem in both the BCS–BEC crossover and strong-coupling regions.

Naturally, no universal dependences on disorder were obtained for the two-particle properties like optical conductivity, where vertex corrections due to disorder scattering become very important, leading to new physics, like that of Anderson transition.

Overall, using the DMFT+ Σ approximation to analyze the disorder effects in the Hubbard model was shown to produce reasonable results for the phase diagram in the repulsive case, as compared to exact numerical simulations of disorder in DMFT, the behavior of the density of states and optical conductivity in both repulsive and attractive cases. However, the role of approximations made in DMFT+ Σ , such as the neglect of the interference of disorder scattering and correlation effects, deserves further studies.

It is a pleasure and honor to dedicate this short review to Professor Leonid Keldysh' 85th birthday. This work is supported by the RSF grant № 14-12-00502.

REFERENCES

1. N. F. Mott, *Metal–Insulator Transitions*, 2nd edn. Taylor and Francis, London (1990).
2. J. Hubbard, Proc. Roy. Soc. London Ser. A **276**, 238 (1963); Proc. Roy. Soc. London Ser. A **277**, 237 (1964); Proc. Roy. Soc. London Ser. A **281**, 401 (1964); Proc. Roy. Soc. London Ser. A **285**, 542 (1965); Proc. Roy. Soc. London Ser. A **296**, 829 (1967); Proc. Roy. Soc. London Ser. A **296**, 100 (1967).
3. W. Metzner and D. Vollhardt, Phys. Rev. Lett. **62**, 324 (1989).
4. D. Vollhardt, in: *Correlated Electron Systems*, ed. by V. J. Emery, World Scientific, Singapore (1993), p. 57.
5. Th. Pruschke, M. Jarrell, and J. K. Freericks, Adv. Phys. **44**, 210 (1995).
6. A. Georges, G. Kotliar, W. Krauth, and M. J. Rozenberg, Rev. Mod. Phys. **68**, 13 (1996).
7. D. Vollhardt, AIP Conf. Proceed. **1297**, 339 (2010); arXiv:1004.5069.
8. G. Kotliar and D. Vollhardt, Physics Today **57**, 53 (2004).
9. D. M. Eagles, Phys. Rev. **186**, 456 (1969).
10. A. J. Leggett, in: *Modern Trends in the Theory of Condensed Matter*, ed. by A. Pekalski and J. Przystawa, Springer, Berlin (1980).
11. P. Nozieres and S. Schmitt-Rink, J. Low Temp. Phys. **59**, 195 (1985).

12. I. Bloch, J. Dalibard, and W. Zwerger, *Rev. Mod. Phys.* **80**, 885 (2008).
13. L. P. Pitaevskii, *Usp. Fiz. Nauk* **176**, 345 (2006) [*Physics Uspekhi* **44**, 333 (2006)].
14. E. Z. Kuchinskii, I. A. Nekrasov, and M. V. Sadovskii, *Pis'ma v ZhETF* **82**, 217 (2005) [*JETP Lett.* **82**, 198 (2005)].
15. M. V. Sadovskii, I. A. Nekrasov, E. Z. Kuchinskii, Th. Pruschke, and V. I. Anisimov, *Phys. Rev. B* **72**, 155105 (2005).
16. E. Z. Kuchinskii, I. A. Nekrasov, and M. V. Sadovskii, *Fiz. Nizk. Temp.* **32**, 528 (2006) [*Low Temp. Phys.* **32**, 398 (2006)].
17. E. Z. Kuchinskii, I. A. Nekrasov, and M. V. Sadovskii, *Usp. Fiz. Nauk* **182**, 345 (2012) [*Physics Uspekhi* **55**, 325 (2012)].
18. E. Z. Kuchinskii, I. A. Nekrasov, and M. V. Sadovskii, *ZhETF* **133**, 670 (2008) [*JETP* **106**, 581 (2008)].
19. E. Z. Kuchinskii, N. A. Kuleeva, I. A. Nekrasov, and M. V. Sadovskii, *ZhETF* **137**, 368 (2010) [*JETP* **110**, 325 (2010)].
20. E. Z. Kuchinskii, I. A. Nekrasov, and M. V. Sadovskii, *Phys. Rev. B* **80**, 115124 (2009).
21. E. Z. Kuchinskii, I. A. Nekrasov, and M. V. Sadovskii, *Phys. Rev. B* **75**, 115102 (2007).
22. N. A. Kuleeva, E. Z. Kuchinskii, and M. V. Sadovskii, *ZhETF* **146**, 304 (2014) [*JETP* **119**, 264 (2014)].
23. E. Z. Kuchinskii, N. A. Kuleeva, and M. V. Sadovskii, *Pis'ma v ZhETF* **100**, 213 (2014) [*JETP Lett.* **100**, 192 (2014)].
24. E. Z. Kuchinskii, N. A. Kuleeva, and M. V. Sadovskii, *ZhETF* **147**, No. 6 (2015) [*JETP* **120**, No. 6 (2015)]; arXiv:1411.1547.
25. P. W. Anderson, *Phys. Rev.* **109**, 1492 (1958).
26. M. V. Sadovskii, *Diagrammatics*, World Scientific, Singapore (2006).
27. R. Bulla, T. A. Costi, and T. Pruschke, *Rev. Mod. Phys.* **60**, 395 (2008).
28. D. Vollhardt and P. Wölfle, *Phys. Rev. B* **22**, 4666 (1980); *Phys. Rev. Lett.* **48**, 699 (1982); in *Anderson Localization*, ed. by Y. Nagaoka and H. Fukuyama, *Springer Series in Solid State Sciences*, Springer-Verlag, Berlin (1982), Vol. 39, p. 26.
29. M. V. Sadovskii, *The Theory of Electron Localization in Disordered Systems. Soviet Scientific Reviews—Physics Reviews*, ed. by I. M. Khalatnikov, Vol. 7, p. 1. Harwood Academic Publ., New York (1986); A. V. Myasnikov and M. V. Sadovskii. *Fiz. Tverd. Tela* **24**, 3569 (1982) [*Sov. Phys.—Solid State* **24**, 2033 (1982)]; E. A. Kotov and M. V. Sadovskii. *Zs. Phys. B* **51**, No. 1, 17 (1983).
30. P. Wölfle and D. Vollhardt, in: *Electronic Phase Transitions*, ed. by W. Hanke and Yu. V. Kopayev, North-Holland, Amsterdam (1992), p. 1.
31. K. Byczuk, W. Hofstetter, and D. Vollhardt, *Phys. Rev. Lett.* **94**, 056404 (2005).
32. R. Bulla, *Phys. Rev. Lett.* **83**, 136 (1999); R. Bulla, T. A. Costi, and D. Vollhardt. *Phys. Rev. B* **64**, 045103 (2001).
33. N. Blümer, *Mott–Hubbard Metal–Insulator Transition and Optical Conductivity*, Thesis, München (2002).
34. P. A. Lee and T. V. Ramakrishnan, *Rev. Mod. Phys.* **57**, 287 (1985); D. Belitz and T. R. Kirkpatrick, *Rev. Mod. Phys.* **66**, 261 (1994).
35. A. M. Finkelshtein, *ZhETF* **84**, 168 (1983) [*Sov. Phys. JEPT* **57** 97 (1983)]; C. Castellani et al., *Phys. Rev. B* **30**, 527 (1984).
36. M. A. Erkabaev and M. V. Sadovskii, *J. Moscow Phys. Soc.* **2**, 233 (1992).
37. M. Keller, W. Metzner, and U. Schollwöck, *Phys. Rev. Lett.* **86**, 4612 (2001).
38. A. Toschi, P. Barone, M. Capone, and C. Castellani, *New J. Phys.* **7**, 7 (2005).
39. J. Bauer, A. C. Hewson, and N. Dupis, *Phys. Rev. B* **79**, 214518 (2009).
40. A. Koga and P. Werner, *Phys. Rev. A* **84**, 023638 (2011).
41. M. V. Sadovskii, *Superconductivity and Localization*, World Scientific, Singapore (2000).
42. P. G. De Gennes, *Superconductivity of Metals and Alloys*, W. A. Benjamin, New York (1966).